

## Measurement of the Tensor Analyzing Powers $T_{20}$ and $T_{21}$ in Elastic Electron-Deuteron Scattering

D. M. Nikolenko,<sup>1</sup> H. Arenhövel,<sup>2</sup> L. M. Barkov,<sup>1</sup> S. L. Belostotsky,<sup>3</sup> V. F. Dmitriev,<sup>1</sup> M. V. Dyug,<sup>1</sup> R. Gilman,<sup>4,5</sup> R. J. Holt,<sup>6</sup> L. G. Isaeva,<sup>1</sup> C. W. de Jager,<sup>7,5</sup> E. R. Kinney,<sup>8</sup> R. S. Kowalczyk,<sup>6</sup> B. A. Lazarenko,<sup>1</sup> A. Yu. Loginov,<sup>9</sup> S. I. Mishnev,<sup>1</sup> V. V. Nelyubin,<sup>3</sup> A. V. Osipov,<sup>9</sup> D. H. Potterveld,<sup>6</sup> I. A. Rachek,<sup>1</sup> R. Sh. Sadykov,<sup>1</sup> Yu. V. Shestakov,<sup>1</sup> A. A. Sidorov,<sup>9</sup> V. N. Stibunov,<sup>9</sup> D. K. Toporkov,<sup>1</sup> V. V. Vikhrov,<sup>3</sup> H. de Vries,<sup>7</sup> and S. A. Zevakov<sup>1</sup>

<sup>1</sup>*Budker Institute for Nuclear Physics, 630090 Novosibirsk, Russia*

<sup>2</sup>*Institut für Kernphysik, Johannes Gutenberg-Universität, D-55099 Mainz, Germany*

<sup>3</sup>*St. Petersburg Nuclear Physics Institute, Gatchina 188350, Russia*

<sup>4</sup>*Rutgers University, Piscataway, New Jersey 08855*

<sup>5</sup>*Thomas Jefferson National Accelerator Facility, Newport News, Virginia 23606*

<sup>6</sup>*Argonne National Laboratory, Argonne, Illinois 60439-4843*

<sup>7</sup>*NIKHEF, P.O. Box 41882, 1009 DB Amsterdam, The Netherlands*

<sup>8</sup>*Colorado University, Boulder, Colorado 80309*

<sup>9</sup>*Nuclear Physics Institute at Tomsk Polytechnical University, 634050 Tomsk, Russia*

(Received 26 August 2002; published 21 February 2003)

The tensor analyzing power components  $T_{20}$  and  $T_{21}$  have been measured in elastic electron-deuteron scattering at the 2 GeV electron storage ring VEPP-3, Novosibirsk, in a four-momentum transfer range from 8.4 to 21.6 fm<sup>-2</sup>. A new polarized internal gas target with an intense cryogenic atomic beam source was used. The new data determine the deuteron form factors  $G_C$  and  $G_Q$  in an important range of momentum transfer where the first node of the deuteron monopole charge form factor is located. The new results are compared with previous data and with some theoretical predictions.

DOI: 10.1103/PhysRevLett.90.072501

PACS numbers: 25.30.Bf, 13.40.Gp, 21.45.+v, 29.25.Pj

Theoretical and experimental investigation of the simplest nucleus, the deuteron, has an important role for the determination of the properties of the nucleon-nucleon interaction as well as for the study of non-nucleonic degrees of freedom. The relationship of these properties to experimental observables is especially clear in elastic electron-deuteron scattering where the theoretical description in terms of form factors is well known, and obscuring effects are small because the electromagnetic force is relatively weak [1,2].

Assuming  $P$  and  $T$  invariance, the electromagnetic structure of the deuteron is completely described by three

form factors: charge monopole  $G_C(Q^2)$ , charge quadrupole  $G_Q(Q^2)$ , and magnetic dipole  $G_M(Q^2)$ . Two deuteron structure functions,  $A = G_C^2 + (8/9)\eta^2 G_Q^2 + (2/3)\eta G_M^2$  and  $B = (4/3)\eta(1 + \eta)G_M^2$  (here  $\eta = Q^2/4M_d^2$ ,  $M_d$  is the deuteron mass, and  $Q$  is the four-momentum transfer), can be derived through measurements of spin-averaged elastic electron-deuteron scattering cross sections ( $\sigma_0$ ). The form factors  $G_C$  and  $G_Q$  can be determined separately only through the additional measurement of a polarization observable. The ratio of the cross section with a tensor-polarized deuteron target [3] to  $\sigma_0$  can be written as

$$\frac{\sigma}{\sigma_0} = 1 + (P_{zz}/\sqrt{2}) \left( \frac{3 \cos^2 \theta^* - 1}{2} T_{20} - \sqrt{\frac{3}{2}} \sin 2\theta^* \cos \phi^* T_{21} + \sqrt{\frac{3}{2}} \sin^2 \theta^* \cos 2\phi^* T_{22} \right) \equiv 1 + (P_{zz}/\sqrt{2}) \sum_{i=0}^2 d_{2i} T_{2i}. \quad (1)$$

Here,  $P_{zz}$  is the degree of deuteron tensor polarization, and the angles  $\theta^*$  and  $\phi^*$  define the polarization orientation in a frame where the  $z$  axis is along the virtual photon direction and the  $x$  axis is in the scattering plane. The tensor analyzing power components can be expressed as

$$T_{20} = -(\sqrt{2}\eta/3S) \left[ 4G_C G_Q + \frac{4\eta}{3} G_Q^2 + \left( \frac{1}{2} + \varepsilon \right) G_M^2 \right],$$

$$T_{21} = \frac{2}{S} \sqrt{\frac{\eta^3(1+\varepsilon)}{3}} G_Q G_M, \quad T_{22} = [\eta/(2\sqrt{3}S)] G_M^2, \quad (2)$$

where  $\varepsilon = (1 + \eta) \tan^2(\theta_e/2)$ ,  $\theta_e$  is the electron scattering angle, and  $S \equiv A + \tan^2(\theta_e/2)B$ .

In previous experiments, the polarization observables were measured by various techniques: polarimeters of recoil deuterons (with both electron beam and target unpolarized) [4–6], polarized internal gas targets in a storage ring (electron beam unpolarized) [7–10], and one experiment with a polarized solid target [11]. Here, we present the results of a measurement performed at the electron storage ring VEPP-3, Novosibirsk, using an internal polarized deuterium gas target.

For the present experiment, a new cryogenic atomic beam source (ABS) [12,13] was implemented. The main difference of this ABS from other modern sources is the use of strong superconducting sextupole magnets instead

of permanent ones; our ABS provides a record flux of  $8.2 \times 10^{16}$  atoms/s (in the three deuteron substates). During the experiment, the sign of the deuteron beam tensor polarization was changed regularly every 30 s. The tensor polarization of the atoms was  $P_{zz}^+ \approx 1$  or  $P_{zz}^- \approx -2$ , while the vector polarization was zero.

The polarized beam from the ABS was injected into an open-ended, T-shaped storage cell with elliptical cross section measuring  $13 \times 24$  mm. This is smaller than that of [8], resulting in an increased target density. The small size was made possible by a modification of the VEPP-3 optics. Cooling the cell with liquid nitrogen further increased the density to achieve an estimated target thickness of  $\sim 8 \times 10^{13}$  atoms/cm<sup>2</sup>. The inner surface of the cell was coated with drifilm to inhibit atom depolarization during collisions with the cell walls.

The polarization of the ABS beam was usually very high ( $\approx 98\%$ ). However, depolarization effects [13] decreased the polarization of the deuterium atoms inside the target cell. The target polarization was determined with the low- $Q$  polarimeter (LQP), which measured the target asymmetry in elastic  $e$ - $d$  scattering at a small momentum transfer,  $Q^2 \approx 2.6$  fm<sup>-2</sup>.

The target asymmetry is defined as (left formula)

$$A^t = \sqrt{2} \frac{(N^+ - N^-)}{(N^- P_{zz}^+ - N^+ P_{zz}^-)}; \quad A^t = \sum_{i=0}^2 d_{2i} T_{2i}, \quad (3)$$

where  $N^+$  and  $N^-$  are the event counts of a detector when the target polarization is  $P_{zz}^+$  and  $P_{zz}^-$ , respectively.  $N^+$  and  $N^-$  are normalized to the electron beam charge. In accordance with Eq. (1),  $A^t$  can be written as a linear combination of tensor analyzing powers (right formula). We assume that depolarization processes occur identically in both polarization states; therefore  $P_{zz}^-/P_{zz}^+$  is close to  $-2$  (the same as for the ABS beam; see also [9]).

The value of  $A^t$  measured by the LQP can be used to calculate the target polarization if the tensor analyzing power is known at small  $Q^2$ . At present, the measurements of  $T_{20}$  (the main contribution to  $A^t$ ) in the LQP  $Q^2$  region are not sufficiently accurate [4,9]. However, at small momentum transfer  $T_{20}$  should be close to its first term in an expansion in powers of  $Q^2$ :  $T_{20} \approx -(\sqrt{2}/3)Q_d \cdot Q^2$ . Here,  $Q_d$  is the deuteron static quadrupole moment. The spread in theoretical predictions for  $T_{20}$  at small  $Q^2$  is small ( $\pm 2\%$ – $3\%$ ) if one considers only those models which predict a value of  $Q_d$  close to the known one. We have employed one such prediction [14] in determining the target polarization.

The average degree of target polarization during the experiment was found to be  $P_{zz}^+ = 0.397 \pm 0.013 \pm 0.018 \pm 0.012$  where the first uncertainty is statistical and the second is systematic. The third is an estimate of the uncertainty in the theoretical prediction. The dominant contributions to the systematic uncertainty come from uncertainties of detector geometry and magnetic holding field direction.

The direction of the deuteron polarization axis was fixed by a magnetic holding field  $\vec{H}$  (the magnet is described in [15]) with  $\theta_{\vec{H}} \approx 120^\circ$  and  $\phi_{\vec{H}} \approx 0^\circ$ ; these angles are defined in a frame where the  $z$  axis is along the direction of the electron beam and the  $x$  axis is directed up. The magnitude of  $\vec{H}$  varied along the storage cell within the interval 88–95 mT, which does not contain any values of  $\vec{H}$  corresponding to depolarizing resonances induced by the electron beam [16].

Large-acceptance nonmagnetic particle detectors were composed of two nearly identical systems. Each consisted of electron and deuteron arms to detect a scattered electron and recoil deuteron in coincidence. The angular acceptance of electron arm 1 was  $\theta_e \approx 16^\circ$ – $30^\circ$ , while  $\phi_e$  ranged from  $-30^\circ$  to  $30^\circ$ ; electron arm 2 used the same angular ranges but the central  $\phi_e$  was  $180^\circ$  ( $\theta_e$  and  $\phi_e$  are in the frame defined above for  $\theta_{\vec{H}}$  and  $\phi_{\vec{H}}$ ). The positions of the deuteron arms were conjugate to the electron ones. The particle trajectories were reconstructed by means of tracking information from different sets of drift chambers. Each electron arm had a segmented CsI + NaI electron calorimeter for measurement of electron energy [17]. The hadron arms were equipped with scintillation hodoscopes, each having three layers of plastic scintillators. The scintillators were used for deuteron energy measurement and for particle identification.

The cross section for elastic  $e$ - $d$  scattering is much smaller than that for proton emission. Deuterons were distinguished from protons by  $E$ - $\Delta E$  and time of flight methods to remove most of the background. Cuts on three kinematic correlations were employed to select elastic scattering events: scattering angle versus deuteron energy, ( $e$ - $d$ ) polar angle, and ( $e$ - $d$ ) azimuthal angle. The residual background was estimated from the azimuthal angle correlation after applying all other cuts. Elastic events clustered in a narrow peak on top of a broad background constituting between  $3.0\% \pm 1.5\%$  (high  $Q^2$  region) to  $8\% \pm 2\%$  (low  $Q^2$  region) of the accepted events.

For arm 1, the direction of the recoil deuteron was almost antiparallel to the polarization axis. In this case, the target asymmetry [see Eq. (3)] depends mainly on the analyzing power  $T_{20}$  [Eq. (1)]. At the same time, for arm 2 the contribution of  $T_{20}$  to  $A^t$  is small, and it depends mainly on  $T_{21}$ .

The range of  $\theta_e$  accepted by the detectors was divided into bins centered at  $16.8^\circ$ ,  $18.3^\circ$ ,  $20.1^\circ$ ,  $22.5^\circ$ ,  $25.1^\circ$ , and  $28.1^\circ$ , with  $Q^2$  of 8.41, 9.88, 11.78, 14.50, 17.67, and 21.56 fm<sup>-2</sup> for the 2 GeV beam energy. Values of  $A^t$  were determined for each bin, and linear equations for  $T_{20}$  and  $T_{21}$  were found and solved, after taking into account the detector solid angle, target density distribution, direction of the magnetic holding field, magnitude of the target polarization, and small contributions of  $T_{22}$  to  $A^t$ .

The results for  $T_{20}$  and  $T_{21}$  as well as statistical and systematic uncertainties are presented in Table I. The

TABLE I.  $T_{20}$  and  $T_{21}$ , obtained in the present experiment; the deuteron form factors  $G_C$  and  $G_Q$  are calculated from the present data and the structure functions  $A$  and  $B$ . The upper errors of  $T_{20}$  and  $T_{21}$  are statistical; the lower ones are systematic.  $Q^2$  is in  $\text{fm}^{-2}$  (see text for corresponding  $\theta_e$ ).

$Q^2$	$T_{20}$	$T_{21}$	$G_C$	$G_Q$
8.41	$-1.294^{+0.084}_{-0.088}$	$0.234^{+0.093}_{-0.022}$	$0.0403^{+0.0046}_{-0.0082}$	$1.772^{+0.320}_{-0.233}$
9.88	$-1.398^{+0.100}_{-0.093}$	$0.318^{+0.086}_{-0.142}$	$0.0257^{+0.0052}_{-0.0018}$	$1.279^{+0.063}_{-0.182}$
11.78	$-1.384^{+0.102}_{-0.092}$	$0.521^{+0.083}_{-0.150}$	$0.0143^{+0.0035}_{-0.0039}$	$0.877^{+0.062}_{-0.077}$
14.50	$-0.982^{+0.169}_{-0.066}$	$0.435^{+0.083}_{-0.111}$	$0.0041^{+0.0032}_{-0.0026}$	$0.549^{+0.017}_{-0.029}$
17.67	$-0.818^{+0.269}_{-0.058}$	$0.808^{+0.279}_{-0.092}$	$0.0011^{+0.0028}_{-0.0023}$	$0.336^{+0.010}_{-0.014}$
21.56	$0.557^{+0.342}_{-0.044}$	$0.299^{+0.410}_{-0.057}$	$-0.0078^{+0.0025}_{-0.0020}$	$0.154^{+0.032}_{-0.037}$

main contributions to the systematic errors of  $T_{20}$  and  $T_{21}$  come from the uncertainties of  $P_{zz}$  (all three errors of  $P_{zz}$  are combined quadratically), the uncertainties in electron and deuteron scattering angles, and the uncertainty in the spin orientation angles.

For comparison of the new data with previous data and theoretical models, small corrections for  $T_{20}$  and for  $T_{21}$  were calculated to adjust them to the conventionally accepted angle of  $\theta_e = 70^\circ$ . These results are presented in Fig. 1. Our results are in agreement with previous measurements. In the region of 8–12  $\text{fm}^{-2}$ , the new results significantly improve the accuracy of  $T_{20}$  and  $T_{21}$ .

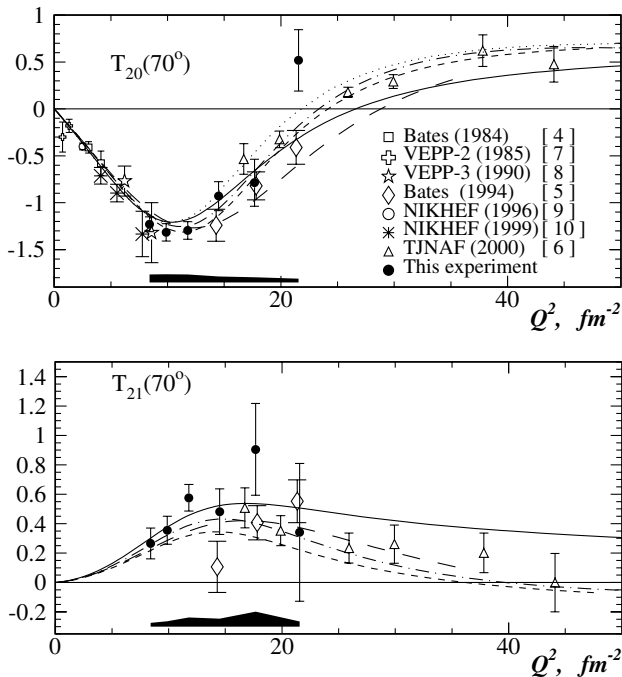


FIG. 1. Experimental results and theoretical predictions for  $T_{20}$  and  $T_{21}$ . The long dashed line is NRIA, Paris potential [18]; nonrelativistic models with relativistic corrections and with MEC contributions are, respectively, the solid [19] and the dotted [20] lines; predictions with relativistic approaches are the dash-dotted [14] and the dashed [21] lines. The shaded area indicates the size of the systematic errors for this experiment.

A comparison of the data for  $T_{20}$  with the prediction of the nonrelativistic impulse approximation (NRIA) with the Paris potential [18] shows that this model does not provide a good description of our data. The nonrelativistic approaches with relativistic corrections and with meson exchange current (MEC) contributions developed in works of Arenhövel *et al.* [19] and Wiringa *et al.* [20] provide better descriptions of  $T_{20}$  data than the previous model. The relativistic models of Phillips *et al.* [14] and Krutov and Troitsky [21] are in good agreement with our data and also [6] at large  $Q^2$ . The prediction [19] for  $T_{21}$  is in good agreement with our data; however, it disagrees with [6]. The models [14,18] are in agreement with [6] and our data, but the prediction [21] disagrees with both. A  $\chi^2$  analysis provides the same conclusions (see Table II). Note that our last experimental bin is always the largest contribution to  $\chi^2$  for  $T_{20}$ .

The form factors  $G_C$  and  $G_Q$  can be extracted from the  $T_{20}$ ,  $A$ , and  $B$  data, but in this case a solution is not unique. As was discussed, for example, in [22], at small  $Q^2$  the physical solution can be selected from the static deuteron moments and can be continued to larger  $Q^2$ . Here, we have found the charge form factors using  $T_{21}$  data as well, performing a minimization of the quantity

$$\chi_G^2 = (G_C^2 + 8/9\eta^2 G_Q^2 - A^*)^2 / \Delta A^{*2} + (G_C G_Q + \eta/3 G_Q^2 - T_{20}^*)^2 / \Delta T_{20}^{*2} + (G_Q - T_{21}^*)^2 / \Delta T_{21}^{*2}. \quad (4)$$

Here,  $A^*$ ,  $T_{20}^*$ , and  $T_{21}^*$  are obtained from measured  $A$ ,  $T_{20}$ , and  $T_{21}$  by transforming them, taking into account the contribution of  $G_M$ .  $G_M$ ,  $A$ , and  $B$  (as well as the values of  $T_{22}$  used above for correcting  $A^*$ ) were obtained from parametrization I [22], which is based on the world data of elastic  $e-d$  scattering. The uncertainties of  $A$  and  $B$  were taken to be the same as in [5]. Here, statistical and systematic uncertainties of  $T_{20}$  and  $T_{21}$  were combined quadratically. Although the  $T_{21}$  data do not, in practice, decrease the errors of  $G_C$  and  $G_Q$ , the minima of  $\chi_G^2$ , corresponding to the physical solutions, become either single or the smaller of two local minima because of the additional information in each of the six bins. Because of the relatively small uncertainties of  $A$ , the uncertainties of  $G_C$  and  $G_Q$  are strongly correlated.

Results obtained for  $G_C$  and  $G_Q$  are presented in Table I and in Fig. 2 together with other data and theoretical

TABLE II. Comparison of the obtained results with theoretical predictions,  $\chi^2/N$  values are presented.

Reference	[18]	[19]	[14]	[21]	[20]
$T_{20}$	3.43	1.87	1.40	1.41	1.49
$T_{21}$	1.59	0.58	1.18	2.25	...
$G_C$	2.88	1.38	0.83	1.83	...
$G_Q$	4.23	7.11	5.21	2.74	...

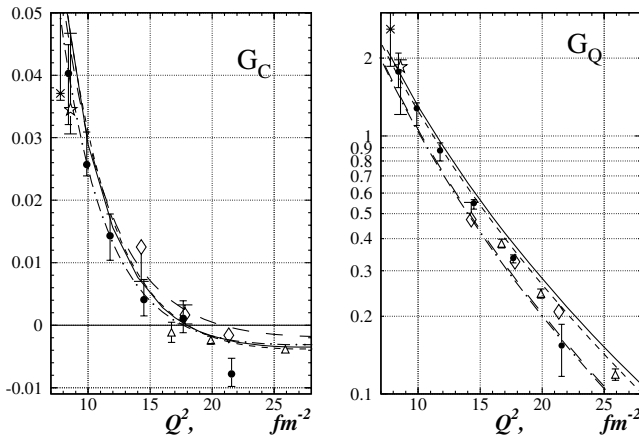


FIG. 2. Experimental results and theoretical predictions for monopole ( $G_C$ ) and quadrupole ( $G_Q$ ) charge form factors of the deuteron. Curves and data are as in Fig. 1.

predictions. One can see that our results agree with, and improve upon, previous data.

Comparison of the present results for  $G_C$  with theoretical models (see Table II) shows a good agreement with the Phillips *et al.* [14] prediction and the greatest difference with the NR1A [18] calculation. The largest contribution in  $\chi^2/N$  comes from our last bin.

For analysis of the  $G_C$  node location we use data in the interval of  $Q^2 = 10\text{--}27\text{ fm}^{-2}$ . Parametrization I [22] was employed; only the node position parameter was varied. The node position from only our data was found at  $16.9^{+1.8}_{-1.0}\text{ fm}^{-2}$ , and from all data ([5,6] and this experiment) was found at  $17.41 \pm 0.32\text{ fm}^{-2}$ .

For  $Q^2 = 14.5$  and  $17.7\text{ fm}^{-2}$ ,  $G_C$  is small and  $A$  is dominated by  $G_Q$ . Hence, the accuracy of  $G_Q$  is high due to the small errors of  $A$ , and a precise check can be made of theoretical predictions. Indeed, these bins give the main contribution to  $\chi^2/N$  for  $G_Q$  shown in Table II. One can see from this table and Fig. 2 that prediction [21] for  $G_Q$  gives the best agreement with data. Note, however, that this comparison does not account for uncertainties of the theoretical models.

In conclusion, the tensor analyzing power components  $T_{20}$  and  $T_{21}$  have been measured in the momentum transfer region of  $8.4\text{--}21.6\text{ fm}^{-2}$ . Our results agree with and improve upon previous data. The deuteron charge form factors  $G_C$  and  $G_Q$  are extracted from our data and  $A$  and  $B$  data in an important range of momentum transfer in which the first node of the monopole form factor is located. Comparison with several theoretical predictions shows a preference for relativistic calculations in describing the whole data set. However, as shown in [2], several relativistic calculations agree with  $T_{20}$  data while their variations for  $A$  and  $B$  are much greater.

We acknowledge the VEPP-3 staff for the stable operation of the storage ring during an almost one-year experi-

ment. We remember with gratitude Stanislav Popov who played a key role in internal target experiments in BINP. The authors are grateful to B. B. Wojtsekhowski, E. P. Tsentalovich, V. Frolov, and D. K. Vesnovski for their contribution in previous phases of the experiment that has an important influence on the present one. We also thank V. A. Elshanski, A. M. Efimov, and A. A. Kovyazin for their help during the experiment. This work was supported by the U.S. Department of Energy under Contract No. W-31-109-ENG-38, by the U.S. National Science Foundation under Grant No. PHY 9803860, by the Russian Foundation for Basic Researches, Grants No. 01-02-17276 and No. 01-02-16929, by INTAS, Grant No. 96-0424, by the Russian Federation Ministry of Education, Grant No. 3-110, and by the State Scientific and Technical Program of Russian Federation.

- [1] M. Garçon and J.W. Van Orden, *Adv. Nucl. Phys.* **26**, 293 (2001).
- [2] R. Gilman and F. Gross, *J. Phys. G* **28**, R37 (2002).
- [3] T.W. Donnelly and A. S. Raskin, *Ann. Phys. (N.Y.)* **169**, 247 (1986).
- [4] M. E. Schulze *et al.*, *Phys. Rev. Lett.* **52**, 597 (1984).
- [5] M. Garçon *et al.*, *Phys. Rev. C* **49**, 2516 (1994).
- [6] D. Abbott *et al.*, *Phys. Rev. Lett.* **84**, 5053 (2000).
- [7] V. F. Dmitriev *et al.*, *Phys. Lett.* **157B**, 143 (1985); B. B. Wojtsekhowski *et al.*, *Pis'ma Zh. Eksp. Teor. Fiz.* **43**, 567 (1986) [*JETP Lett.* **43**, 733 (1986)].
- [8] R. Gilman *et al.*, *Phys. Rev. Lett.* **65**, 1733 (1990).
- [9] M. Ferro-Luzzi *et al.*, *Phys. Rev. Lett.* **77**, 2630 (1996).
- [10] M. Bouwhuis *et al.*, *Phys. Rev. Lett.* **82**, 3755 (1999).
- [11] B. Boden *et al.*, *Z. Phys. C* **49**, 175 (1991).
- [12] L. G. Isaeva *et al.*, *Nucl. Instrum. Methods Phys. Res., Sect. A* **411**, 201 (1998).
- [13] Yu. V. Shestakov *et al.*, Budker Institute for Nuclear Physics Report No. 2001-76, Novosibirsk, 2001.
- [14] D. R. Phillips, S. J. Wallace, and N. K. Devine, *Phys. Rev. C* **58**, 2261 (1998); D. R. Phillips (private communication).
- [15] K. P. Coulter *et al.*, *Nucl. Instrum. Methods Phys. Res., Sect. A* **350**, 423 (1994).
- [16] R. Gilman *et al.*, *Nucl. Instrum. Methods Phys. Res., Sect. A* **327**, 277 (1993).
- [17] J. A. P. Theunissen *et al.*, *Nucl. Instrum. Methods Phys. Res., Sect. A* **348**, 61 (1994).
- [18] M. Lacombe *et al.*, *Phys. Lett.* **101B**, 139 (1981).
- [19] H. Arenhövel, F. Ritz, and T. Wilbois, *Phys. Rev. C* **61**, 034002 (2000); H. Arenhövel (private communication).
- [20] R. B. Wiringa, V. G. J. Stoks, and R. Schiavilla, *Phys. Rev. C* **51**, 38 (1995).
- [21] A. F. Krutov and V. E. Troitsky, hep-ph/0202183; (private communication).
- [22] D. Abbott *et al.*, *Eur. Phys. J. A* **7**, 421 (2000); J. Ball (private communication).